INFLUENCES OF DIFFERENT INTEGRAL KERNELS TO THE SOLUTIONS OF BOUNDARY INTEGRAL EQUATION IN PLANE ELASTICITY

Y. Z. Chen
Division of Engineering Mechanics, Jiangsu University
Zhenjiang, Jiangsu, 212013 P. R. China
* Corresponding author. Tel.: +86 0511 88780780; fax: +86 0511 88791739
E-mail address: chens@ujs.edu.cn

Abstract In addition to the usual integral kernel in BIE, a modified one is introduced. The formulation for modified one is based on a representation in the pure deformable form for the fundamental solution of concentrated forces. It is found that the modified one can be used to any case, even if the loadings on the contour are not in equilibrium in an exterior boundary value problem (BVP). The influences of different integral kernels to solutions of BIE, particularly, in the Neumann problem and the Dirichlet problem are addressed. Numerical examples are presented to prove the assertion proposed. Properties of solutions from the usage of the modified integral kernel are studied in detail. The influences of different integral kernels to the degenerate scale are discussed and numerical results are provided. It is found that the influences of the constant involved in the integral kernels are significant. For the cases of the elliptic and the rectangular contour, the influences to the degenerate scale are studied with numerical results.

Keywords: Boundary integral equation. Exterior boundary value problem. Regularity condition. Numerical method. Degenerate scale problem.

1. Introduction

The boundary integral equation (abbreviated as BIE) was widely used in elasticity, and the fundamental for BIE could be found from [Rizzo 1967; Cruse 1969; Brebbia et al 1984; Jaswon and Symm 1977]. Recently, development of the boundary element method was summarized [Cheng and Cheng 2005].

There are still some problems in the study of BIEs. The first problem is the regularity condition in the exterior boundary value problem [Brebbia et al 1984]. Generally, the Betti's reciprocal theorem or the Somigliana's identity is used for the formulation of the BIE. In the exterior BVP, if a mutual work difference integral (abbreviated as MWDI) on a sufficient large circle vanishes, the regularity

condition is satisfied. However, this condition has not been studied clearly. Once the BIE in plane elasticity is formulated for the exterior region, one must meet a term called the MWDI , or the terms $D^{*1}_{i(CR)}(\xi)$ or $D^{*2}_{i(CR)}(\xi)$ in Eqs. (8) and (18) used below. If the MWDI vanishes, the regularity condition at infinity is satisfied. In fact, the MWDI is a difference of two works, which are defined by the works done by the fundamental field to the physical stress field each other. Therefore, the property of the MWDI depends on the representation of the fundamental field and the property of the physical stress field. A general expression for the MWDI from two stress fields was obtained in [Chen 2003]. This will be a theoretical basis in the present study.

In fact, it has been proved if the loadings applied on the contour in the exterior BVP are not in equilibrium, instead of using the usual integral kernel $U^{*2}_{ij}(\xi, x)$ (see Eq. (15) below) one should use the modified one $U^{*1}_{ij}(\xi, x)$ (see Eq. (6) below). Two integral kernels have a difference of constant. Clearly, two different integral kernels, the $U^{*1}_{ij}(\xi, x)$ and the $U^{*2}_{ij}(\xi, x)$, will influence the properties of solutions obtained.

The second problem in this field is the degenerate scale problem [Chen et al. 2005; He et al. 1996; Vodicka and Mantic 2008; Chen et al. 2002; Chen and Shen 2007]. In the degenerate scale problem, an improper solution in the Dirichlet problem of BIE exists if the used size is near the critical value. Clearly, the degenerate scale for the individual problem must depend on the used integral kernels, for example the $U^{*1}_{ij}(\xi, x)$ and the $U^{*2}_{ij}(\xi, x)$. This problem was also not investigated in detail previously.

In this paper, in addition to the usual integral kernel $U^{*2}_{ij}(\xi, x)$ (see Eq. (15) below), the modified one, or $U^{*1}_{ij}(\xi, x)$ (see Eq. (6)) is introduced. The formulation for modified one is based on a representation in the pure deformable form for the fundamental solution of concentrated forces. The two kernels $U^{*1}_{ij}(\xi, x)$ and $U^{*2}_{ij}(\xi, x)$ have a difference of constant. It is found that the modified one, or $U^{*1}_{ij}(\xi, x)$, can be used to any case, even if the loadings on the contour are not in equilibrium in an exterior BVP. The influences of different integral kernels to solutions of BIE, particularly in the

Neumann problem and the Dirichlet problem, are addressed. The properties of solution by using $U_{ij}^{*1}(\xi, x)$ are discussed in detail. Numerical examples are presented to prove the assertion proposed. The influences from the used integral kernels to the degenerate scale are discussed and numerical results are provided. It is found that the influences of the constant in the integral kernels to the degenerate scale are significant. For the cases of elliptic and rectangular contour, the influences are studied with numerical results.

2. Influences of different kernels to the solutions of exterior boundary integral equation

2.1 Formulation of two kernels $U_{ij}^{*1}(\xi, x)$, $U_{ij}^{*2}(\xi, x)$ and the relevant boundary integral equations

The following analysis depends on the complex variable function method in plane elasticity [Muskhelishvili 1953]. In the method, the stresses ($\sigma_x, \sigma_y, \sigma_{xy}$), the resultant forces (X, Y) and the displacements (u, v) are expressed in terms of two complex potentials $\phi(z)$ and $\psi(z)$ such that

$$\sigma_x + \sigma_y = 4\,\mathrm{Re}\,\phi'(z)$$

$$\sigma_y - \sigma_x + 2i\sigma_{xy} = 2[\bar{z}\phi''(z) + \psi'(z)] \tag{1}$$

$$f = -Y + iX = \phi(z) + z\overline{\phi'(z)} + \overline{\psi(z)} \tag{2}$$

$$2G(u + iv) = \kappa\phi(z) - z\overline{\phi'(z)} - \overline{\psi(z)} \tag{3}$$

where z=x+iy denotes complex variable, G is the shear modulus of elasticity, $\kappa = (3-\nu)/(1+\nu)$ is for the plane stress problems, $\kappa = 3 - 4\nu$ is for the plane strain problems, and ν is the Poisson's ratio. In the present study, the plane strain condition is assumed thoroughly. In the following, we occasionally rewrite the displacements "u", "v" as u_1, u_2, $\sigma_x, \sigma_y, \sigma_{xy}$ as $\sigma_{11}, \sigma_{22}, \sigma_{12}$, and "x", "y" as x_1, x_2, respectively.

It is emphasized here that we only consider the exterior BVP. Secondly, the remote tractions σ_x^{∞}, σ_y^{∞} and σ_{xy}^{∞} are assumed to tend to zero in this study, or $\sigma_x^{\infty} \to 0$, $\sigma_y^{\infty} \to 0$ and $\sigma_{xy}^{\infty} \to 0$.

The formulation of BIE is introduced below. If the concentrated forces (P_x , P_y) is applied at the point z=t (Fig. 1(a)) , the relevant complex potentials are defined by [Muskhelishvili 1953]

$$\phi_{(\alpha)}(z) = F\ln(z-t)\,,\ \psi_{(\alpha)}(z) = -\kappa\bar{F}\ln(z-t) - \frac{F\bar{t}}{z-t} \tag{4}$$

where

$$F = -\frac{P_x + iP_y}{2\pi(\kappa+1)} \tag{5}$$

In Eq. (4), the subscript "(α)" denotes the fundamental solution initiated by concentrated forces. Note that the relevant complex potentials shown by Eq. (4) are expressed in a pure deformable form [Chen and Lin 2008].

A direct substitution from the complex potentials shown by Eq. (4) in the proper place will lead to the following kernel [Chen and Lin 2008]

$$U_{ij}^{*1}(\xi, x) = \frac{1}{8\pi(1-v)G}\left\{-(3-4v)\ln(r)\delta_{ij} + r_{,i}r_{,j} - 0.5\delta_{ij}\right\} \tag{6}$$

which is used in a BIE mentioned below.

Without losing generality, we can introduce the BIE for the region between the elliptic contour "Γ"and a large circle "CR" (Fig. 1(b)). The observation point "ξ "is assumed on the elliptic contour $\xi \in \Gamma$. For the plane strain case, the suggested BIE can be written as follows [Brebbia et al 1984]

$$\frac{1}{2}u_i(\xi) + \int_\Gamma P_{ij}^*(\xi, x)u_j(x)ds(x) = \int_\Gamma U_{ij}^{*1}(\xi, x)p_j(x)ds(x) + D_{i(CR)}^{*1}(\xi)\ \text{, (i=1,2}\ \xi \in \Gamma\text{)} \tag{7}$$

where $D_{i(CR)}^{*1}(\xi)$ is a mutual work difference integral (abbreviated as MWDI) on a large circle "CR" and is defined by

$$D_{i(CR)}^{*1}(\xi) = -\int_{CR} P_{ij}^*(\xi, x)u_j(x)ds(x) + \int_{CR} U_{ij}^{*1}(\xi, x)p_j(x)ds(x)\text{ , (i=1,2}\ \xi \in \Gamma\text{)} \tag{8}$$

In Eq. (8), "CR" denotes a sufficient large circle with a radius "R".

In addition, the kernel $P_{ij}^*(\xi, x)$ is defined by [Brebbia et al 1984]

$$P_{ij}^*(\xi, x) = -\frac{1}{4\pi(1-v)}\frac{1}{r}\left\{(r_{,1}n_1 + r_{,2}n_2)((1-2v)\delta_{ij} + 2r_{,i}r_{,j}) + (1-2v)(n_i r_{,j} - n_j r_{,i})\right\} \tag{9}$$

where Kronecker deltas δ_{ij} is defined as, $\delta_{ij}=1$ for i=j, $\delta_{ij}=0$ for $i\neq j$, and

$$r_{,1}=\frac{x_1-\xi_1}{r}=\cos\alpha\,,\qquad r_{,2}=\frac{x_2-\xi_2}{r}=\sin\alpha \tag{10}$$

$$n_1=-\sin\beta\,,\quad n_2=\cos\beta \tag{11}$$

where the angles "α" and "β" are indicated in Fig. 1.

Even the physical field is caused by a non- equilibrium force on the elliptic contour, we have proved that $D^{*1}_{i(CR)}(\xi)=0$ (i=1,2) [Chen and Lin 2008]

$$D^{*1}_{i(CR)}(\xi)=-\int_{CR}P^{*}_{ij}(\xi,x)u_j(x)ds(x)+\int_{CR}U^{*1}_{ij}(\xi,x)p_j(x)ds(x)=0\,,\ (i=1,2\ \xi\in\Gamma) \tag{12}$$

Therefore, Eq. (7) can be reduced into

$$\frac{1}{2}u_i(\xi)+\int_{\Gamma}P^{*}_{ij}(\xi,x)u_j(x)ds(x)=\int_{\Gamma}U^{*1}_{ij}(\xi,x)p_j(x)ds(x)\ ,\ (i=1,2\ \xi\in\Gamma) \tag{13}$$

It is emphasized here that the displacements $u_j(x)$ in the left hand side of Eq. (13) should be expressed in the pure deformable form.

In addition, if the same concentrated forces (P_x , P_y) is applied at the point z=t (Fig. 1(a)) , the relevant complex potentials can be defined alternatively by [Muskhelishvili 1953]

$$\phi_{(\alpha)}(z)=F\ln(z-t)\,,\ \psi_{(\alpha)}(z)=-\kappa\bar{F}\ln(z-t)-\frac{F\bar{t}}{z-t}+\bar{F} \tag{14}$$

The complex potentials shown by Eq. (14) are different with those shown by Eq. (4) by a constant $\bar{F}$ in the function $\psi_{(\alpha)}(z)$.

Comparing Eq. (4) with Eq. (14), an additional pair of the complex potentials $\phi(z)=0$, $\psi(z)=\bar{F}$ is presented in Eq. (14). Clearly, this pair causes no stresses anywhere, and represents a rigid translation. Therefore, it is said that the complex potentials shown by Eq. (14) are expressed in an impure deformable form.

A direct substitution from the complex potentials shown by Eq. (14) in the proper place will lead to the following kernel [Chen and Lin 2008]

$$U_{ij}^{*2}(\xi,x)=\frac{1}{8\pi(1-v)G}\left\{-(3-4v)\ln(r)\delta_{ij}+r_{,i}r_{,j}\right\} \quad (15)$$

Note that, the two kernels have the following relation

$$U_{ij}^{*2}(\xi,x)-U_{ij}^{*1}(\xi,x)=\frac{1}{16\pi(1-v)G}\delta_{ij} \quad (16)$$

This kernel $U_{ij}^{*2}(\xi,x)$ was cited in any available textbook [Brebbia et al 1984]. Similarly, from the kernel $U_{ij}^{*2}(\xi,x)$ shown by Eq. (15), the following BIE is obtained

$$\frac{1}{2}u_i(\xi)+\int_\Gamma P_{ij}^*(\xi,x)u_j(x)ds(x)=\int_\Gamma U_{ij}^{*2}(\xi,x)p_j(x)ds(x)+D_{i(CR)}^{*2}(\xi)\ ,\ (i=1,2\ \xi\in\Gamma) \quad (17)$$

where $D_{i(CR)}^{*2}(\xi)$ is a MWDI on a large circle and is defined by

$$D_{i(CR)}^{*2}(\xi)=-\int_{CR}P_{ij}^*(\xi,x)u_j(x)ds(x)+\int_{CR}U_{ij}^{*2}(\xi,x)p_j(x)ds(x)\ ,\ (i=1,2\ \xi\in\Gamma) \quad (18)$$

It was proved that when the physical field is caused by a non- equilibrium force on the elliptic contour, we have $D_{i(CR)}^{*2}(\xi)\neq 0$ (i=1,2) [Chen and Lin 2008]. Thus, in this case, the BIE (17) cannot be reduced further.

It was also proved that when the physical field is caused by an equilibrium force on the elliptic contour, we have $D_{i(CR)}^{*2}(\xi)=0$ (i=1,2) [Chen and Lin 2008]. Thus, in this case, the BIE (17) can be reduced into the following form

$$\frac{1}{2}u_i(\xi)+\int_\Gamma P_{ij}^*(\xi,x)u_j(x)ds(x)=\int_\Gamma U_{ij}^{*2}(\xi,x)p_j(x)ds(x)\ ,\ (i=1,2\ \xi\in\Gamma) \quad (19)$$

In the exterior BVP, it is emphasized here that the BIE with usage of the kernel $U_{ij}^{*1}(\xi,x)$ shown by Eq. (6) can be used to any case even the applied loadings on the elliptic contour are not in equilibrium. However, in the exterior BVP, the BIE with usage of the kernel $U_{ij}^{*2}(\xi,x)$ shown by Eq. (15) can only be used to case that the applied loadings on the elliptic contour are in equilibrium.

2.2 General properties for the solutions from BIE

As claimed previously, the kernel $U_{ij}^{*1}(\xi,x)$ can be used to any case without regarding the loading

condition on the elliptic contour. Therefore, for the exterior boundary value problem the following BIE is suggested

$$\frac{1}{2}u_i(\xi)+\int_\Gamma P_{ij}^*(\xi,x)u_j(x)ds(x)=\int_\Gamma U_{ij}^{*1}(\xi,x)p_j(x)ds(x)\ ,\ (i=1,2\,\xi\in\Gamma) \qquad (13)$$

The problem of equivalence of the solution from BIE and an elasticity solution is studied below. As stated previously, the physical stress field is assumed in the pure deformable form. Therefore, if the $u_i(\xi)$, $u_j(x)$ and $p_j(x)$ in Eq. (13) are some boundary values of an elasticity solution expressed in the pure deformable form, those functions $u_i(\xi)$, $u_j(x)$ and $p_j(x)$ must satisfy the BIE shown by Eq. (13).

In addition, if the $u_i(\xi)$, $u_j(x)$ and $p_j(x)$ in Eq. (13) are some boundary values of an elasticity solution expressed in the impure deformable form, those functions $u_i(\xi)$, $u_j(x)$ and $p_j(x)$ must not satisfy the BIE shown by Eq. (13).

This situation can be seen from the following example. It is known that, there are three particular elasticity solutions, which are as follows

$$\begin{Bmatrix}u_1^{(1)}\\u_2^{(1)}\end{Bmatrix}=\begin{Bmatrix}b_1^{(1)}\\b_2^{(1)}\end{Bmatrix}=\begin{Bmatrix}1\\0\end{Bmatrix},\quad \sigma_{ij}^{(1)}=0 \text{ and } \quad p_i^{(1)}=0 \qquad (20)$$

$$\begin{Bmatrix}u_1^{(2)}\\u_2^{(3)}\end{Bmatrix}=\begin{Bmatrix}b_1^{(2)}\\b_2^{(2)}\end{Bmatrix}=\begin{Bmatrix}0\\1\end{Bmatrix},\quad \sigma_{ij}^{(2)}=0 \text{ and } \quad p_i^{(2)}=0 \qquad (21)$$

$$\begin{Bmatrix}u_1^{(3)}\\u_2^{(3)}\end{Bmatrix}=\begin{Bmatrix}b_1^{(3)}\\b_2^{(3)}\end{Bmatrix}=\begin{Bmatrix}-y_t\\x_t\end{Bmatrix},\ \sigma_{ij}^{(3)}=0 \text{ and } \quad p_i^{(3)}=0 \quad (\ t=x_t+iy_t\in\Gamma) \qquad (22)$$

Clearly, the stress fields shown by Eqs. (20), (21), (22), represent translations or rotation for the body. It has been proved that, substituting those displacements on the contour into left hand term of Eq. (13) yields

$$\left\{\frac{1}{2}u_i(\xi)+\int_\Gamma P_{ij}^*(\xi,x)u_j(x)ds(x)\right\}\Big|_{u_i\to b_i^{(k)}}=b_i^{(k)}\neq 0 \quad (k=1,2,3) \qquad (23)$$

In addition, substituting those tractions $p_j(x)$ on the contour shown by Eqs. (20),(21),(22) into right hand term of Eq. (13) yields

$$\left\{\int_\Gamma U_{ij}^{*1}(\xi,x)p_j(x)ds(x)\right\}\Big|_{p_j\to p_j^{(k)}=0}=0 \tag{24}$$

After comparing Eq. (23) with (24), which are the left and right hand terms of Eq. (13) respectively, the motioned assertion is proved.

In the Neumann problem, the boundary tractions $\tilde{p}_j(x)$ (j=1,2) are given beforehand. Therefore, in the case of using the kernel $U_{ij}^{*1}(\xi,x)$, from Eq. (13) we can obtain the following BIE

$$\frac{1}{2}u_i(\xi)+\int_\Gamma P_{ij}^{*}(\xi,x)u_j(x)ds(x)=g_i(\xi)\ ,\quad (i=1,2,\ \xi\in\Gamma) \tag{25}$$

where

$$g_i(\xi)=\int_\Gamma U_{ij}^{*1}(\xi,x)\tilde{p}_j(x)ds(x)\ ,\quad (i=1,2,\ \xi\in\Gamma) \tag{26}$$

In Eq. (26), $\tilde{p}_j(x)$ (j=1,2) are the boundary tractions which are given beforehand.

It is known that BIE shown by Eq. (25) processes the invertible property. Alternatively speaking, the BIE shown by Eq. (25) can be solved for any right hand term $g_i(\xi)$. However, the obtained $u_j(x)$ (j=1,2) belong to some boundary values of displacements in an elasticity solution expressed in the pure deformable form.

Similarly, in the Dirichlet problem, the boundary displacements $\tilde{u}_j(x)$ (j=1,2) are given beforehand. Therefore, in the case of using the kernel $U_{ij}^{*1}(\xi,x)$, from Eq. (13) we can obtain the following BIE

$$\int_\Gamma U_{ij}^{*1}(\xi,x)p_j(x)ds(x)=h_i(\xi)\ ,\quad (i=1,2,\ \xi\in\Gamma) \tag{27}$$

where

$$h_i(\xi)=\frac{1}{2}\tilde{u}_i(\xi)+\int_\Gamma P_{ij}^{*}(\xi,x)\tilde{u}_j(x)ds(x)\ ,\quad (i=1,2,\ \xi\in\Gamma) \tag{28}$$

In Eq. (28), $\tilde{u}_i(\xi)$ (i=1,2) and $\tilde{u}_j(x)$ (j=1,2) are the boundary displacements, which are given beforehand.

It is known that BIE shown by Eq. (27) processes the invertible property only if the degenerate scale has not been reached [Vodicka and Mantic 2008]. Alternatively speaking, the BIE shown by Eq.

(27) can be solved for any right hand term $h_i(\xi)$ only if the degenerate scale has not been reached. However, the obtained $p_j(x)$ (j=1,2) belong to some boundary values of tractions in an elasticity solution. Generally, those tractions or $p_j(x)$ (j=1,2) may have a resultant force along the contour.

2.3 Numerical examinations for two kernels $U_{ij}^{*1}(\xi,x)$ and $U_{ij}^{*2}(\xi,x)$ in the case of non-equilibrium loadings on the contour

In order to examine the behavior of the kernels $U_{ij}^{*1}(\xi,x)$ and $U_{ij}^{*2}(\xi,x)$, the relevant BIEs are written below

$$\frac{1}{2}u_i(\xi)+\int_\Gamma P_{ij}^*(\xi,x)u_j(x)ds(x)=\int_\Gamma U_{ij}^{*1}(\xi,x)p_j(x)ds(x)\ ,\quad (i=1,2\ \xi\in\Gamma) \qquad (13)$$

$$\frac{1}{2}u_i(\xi)+\int_\Gamma P_{ij}^*(\xi,x)u_j(x)ds(x)=\int_\Gamma U_{ij}^{*2}(\xi,x)p_j(x)ds(x)\ ,\quad (i=1,2\ \xi\in\Gamma) \qquad (19)$$

In all studied problems below, one knows a closed form solution beforehand. Substituting the results from the known solution, for example, for $p_j(x)$ (j=1,2) into right hand term of Eq. (13) will yield a BIE for $u_j(x)$ (j=1,2). The displacements for $u_j(x)$ (j=1,2) can be solved from the BIE. In addition, one compares the obtained displacements $u_j(x)$ (j=1,2) with those from the closed form solution. This will complete the process of comparison. In the solution of BIE, the used scale is assumed to be sufficient large that can avoid coinciding of the used scale to the degenerate scale.

Example 1

The above-mentioned results from theoretical analysis can be examined by the following concrete examples. In the examples, the ellipse has a major half-axis “a” and minor half-axis “b” (Fig. 1(b)). In computation, the plane strain condition and $\nu=0.3$ are assumed. The elliptic contour is divided into 120 intervals. For the BIE solution, the constant displacement and traction are assumed for each interval.

In the example, we propose the following complex potentials

$$\phi(z) = q_o A \ln z \ , \quad \psi(z) = -\kappa q_o \overline{A} \ln z \ , \quad \text{where } A = A_1 + iA_2 \tag{29}$$

where q_o is a unit loading. From complex potentials shown by Eq. (29) and Eq. (2), it is seen that the following resultant forces are applied

$$\{X + iY\}_{re} = -2\pi(\kappa+1)q_o A \tag{30}$$

on the contour. In this case, the exact solution for the displacements and stresses on the boundary contour can easily obtained from Eqs. (1),(3) and (29).

In the Example 1, the examination is performed from the viewpoint of the Neumann problem. The loadings applied on the contour, or p_j (j=1,2) are computed from the complex potentials shown by Eq. (29), and the obtained tractions p_j (j=1,2) are substituted into the right hand term of Eq. (13) (or (19)). Standard numerical technique is used to solve Eq. (13) (or (19)), and the boundary displacements u_j (j=1,2) can be evaluated immediately. The calculated boundary displacements by using the kernels $U_{ij}^{*1}(\xi, x)$ or $U_{ij}^{*2}(\xi, x)$, and those from the exact solution are expressed by

$$u_1 = \frac{q_o}{2G(1+\nu)} f_1(\theta), \quad u_2 = \frac{q_o}{2G(1+\nu)} f_2(\theta), \ (\text{ at the point } x = a\cos\theta, \ y = b\cos\theta \ ) \tag{31}$$

For the case of b/a=0.25 , a=40 , $A_1 = 1$ and $A_2 = 0.5$, the calculated results using the kernels $U_{ij}^{*1}(\xi, x)$ and $U_{ij}^{*2}(\xi, x)$, and the exact results from the closed form solution are shown in Fig. 2, where (a) $f_1(\theta)_{ex}, f_2(\theta)_{ex}$ are from exact solution, or from the complex potentials Eq. (29) directly, (b) $f_1(\theta)_{*1}$ $f_2(\theta)_{*1}$ are from the usage of the kernels $U_{ij}^{*1}(\xi, x)$ and (c) $f_1(\theta)_{*2}$, $f_2(\theta)_{*2}$ are from the usage of the kernels $U_{ij}^{*2}(\xi, x)$.

It is found from Fig. 2 that the computed results for $f_1(\theta)_{*1}$, $f_2(\theta)_{*1}$ from the usage of the kernel $U_{ij}^{*1}(\xi, x)$ are very accurate, which coincide with the results from the exact solution (denoted by $f_1(\theta)_{ex}, f_2(\theta)_{ex}$) . However, the computed results for $f_1(\theta)_{*2}$, $f_2(\theta)_{*2}$ from the usage of the kernel $U_{ij}^{*2}(\xi, x)$ have much difference with those from the exact solution (denoted by $f_1(\theta)_{ex}$, $f_2(\theta)_{ex}$). It is also found that the computed results for $f_1(\theta)_{*2}$, $f_2(\theta)_{*2}$ have a constant difference

from $f_1(\theta)_{ex}$, $f_2(\theta)_{ex}$.

Similarly, in the case of b/a=0.25, a=4, $A_1 = 1$ and $A_2 = 0.5$, the calculated results using the kernels $U_{ij}^{*1}(\xi, x)$ and $U_{ij}^{*2}(\xi, x)$, and the exact results from the closed form solution are shown in Fig. 3. Similar phenomena as in the previous case can be found.

Figs. 2,3

Example 2

All the conditions used in the Example 1 are still used in the present example. However, in the present example, the examination is performed from the viewpoint of the Dirichlet problem. The displacements on the contour, or u_j (j=1,2) are computed from the complex potentials shown by Eq. (29), and the obtained displacements u_j (j=1,2) are substituted into the left hand term of Eqs. (13) (or (19)). Standard numerical technique is used to solve Eq. (13) (or (19)), and the boundary tractions p_j (j=1,2) can be evaluated immediately. The calculated boundary tractions are expressed by

$$p_1 = q_o g_1(\theta), \quad p_2 = q_o g_2(\theta), \quad (\text{at the point } x = a\cos\theta,\ x = b\cos\theta) \qquad (32)$$

For the case of b/a=0.25, a=40, $A_1 = 1$ and $A_2 = 0.5$, the calculated results using the kernels $U_{ij}^{*1}(\xi, x)$ and $U_{ij}^{*2}(\xi, x)$, and the exact results from the closed form solution are shown in Fig. 4, where (a) $g_1(\theta)_{ex}, g_2(\theta)_{ex}$ are from exact solution, or from the complex potentials Eq. (29) directly, (b) $g_1(\theta)_{*1}$ $g_2(\theta)_{*1}$ are from the usage of the kernels $U_{ij}^{*1}(\xi, x)$ and (c) $g_1(\theta)_{*2}$, $g_2(\theta)_{*2}$ are from the usage the kernels $U_{ij}^{*2}(\xi, x)$.

It is found from Fig. 4 that the computed results for $g_1(\theta)_{*1}$ $g_2(\theta)_{*1}$ from the usage of the kernel $U_{ij}^{*1}(\xi, x)$ are very accurate, which coincide with the results from the exact solution (denoted by $g_1(\theta)_{ex}, g_2(\theta)_{ex}$). However, the computed results for $g_1(\theta)_{*2}$, $g_2(\theta)_{*2}$ from the usage of the kernel $U_{ij}^{*2}(\xi, x)$ have much difference with those from the exact solution (denoted by $g_1(\theta)_{ex}$, $g_2(\theta)_{ex}$).

Similarly, in the case of b/a=0.25 , a=4 , $A_1 = 1$ and $A_2 = 0.5$, the calculated results using the kernels $U_{ij}^{*1}(\xi, x)$ and $U_{ij}^{*2}(\xi, x)$, and the exact results from the closed form solution are shown in Fig. 5. Similar results as in previous case have been found. Particularly, in this case, the deviation of the result by usage of the kernel $U_{ij}^{*2}(\xi, x)$ can reach a higher value. For example, in the case of $\theta = \pi$ we have $g_1(\theta)_{ex}$ =-1.195 (from the exact solution), $g_1(\theta)_{*1}$ =-1.200 (by using the kernel $U_{ij}^{*1}(\xi, x)$) $g_1(\theta)_{*2}$ =-2.842 (by using the kernel $U_{ij}^{*2}(\xi, x)$), respectively (Fig. 5).

Figs. 4,5

2.4 Numerical examinations for two kernels $U_{ij}^{*1}(\xi, x)$ and $U_{ij}^{*2}(\xi, x)$ in the case of equilibrium loadings on the contour

As mentioned previously, in the case of equilibrium loadings on the contour, the solutions obtained from two kinds of BIE shown by Eqs. (13) and (19) must be the same. This conclusion is also examined by the following examples.

Example 3

In the example, we propose the following complex potentials

$$\phi(z) = q_o \frac{A}{z}, \quad \psi(z) = q_o \frac{B}{z} \quad \text{where } A = A_1 + iA_2, \ B = B_1 + iB_2 \tag{33}$$

where q_o is a unit loading. From complex potentials shown by Eq. (33) we see that the loadings applied on the contour must be in equilibrium [Muskhelishvili 1953].

Similarly, in the Neumann problem, the calculated boundary displacements by using the kernels $U_{ij}^{*1}(\xi, x)$ or $U_{ij}^{*2}(\xi, x)$, and those from the exact solution are expressed by

$$u_1 = \frac{q_o}{2G(1+\nu)} f_1(\theta), \quad u_2 = \frac{q_o}{2G(1+\nu)} f_2(\theta) \quad (\text{at the point } x = a\cos\theta, \ x = b\cos\theta) \tag{31}$$

For the case of b/a=0.25 , a=40 , $A_1 = 1, A_2 = 0.5$, $B_1 = 1$ and $B_2 = 0.5$ the calculated results using the kernels $U_{ij}^{*1}(\xi, x)$ and $U_{ij}^{*2}(\xi, x)$, and the exact results from the closed form solution are shown in Fig. 6, where (a) $f_1(\theta)_{ex}, f_2(\theta)_{ex}$ are from exact solution, or from the complex potentials

Eq. (33) directly, (b) $f_1(\theta)_{*1}$ $f_2(\theta)_{*1}$ are from the usage of the kernels $U_{ij}^{*1}(\xi, x)$ and (c) $f_1(\theta)_{*2}$, $f_2(\theta)_{*2}$ are from the usage of the kernels $U_{ij}^{*2}(\xi, x)$.

It is found from Fig. 6 that, the computed results from the usage of the kernel $U_{ij}^{*1}(\xi, x)$ or $U_{ij}^{*2}(\xi, x)$, and those from the exact solution, are merged into the same curves.

Example 4

All the conditions used in the Example 3 are still used in the present example. However, in the present example, the examination is performed from the viewpoint of the Dirichlet problem. The displacements on the contour, or u_j (j=1,2) are computed from the complex potentials shown by Eq. (33), and the obtained displacements u_j (j=1,2) are substituted into the left hand term of Eqs. (13) (or (19)). The calculated boundary tractions are expressed by

$$p_1 = q_o g_1(\theta), \quad p_2 = q_o g_2(\theta) \quad (\text{at the point } x = a\cos\theta,\ x = b\cos\theta) \qquad (32)$$

For the case of b/a=0.25, a=40, $A_1 = 1, A_2 = 0.5$, $B_1 = 1$ and $B_2 = 0.5$ the calculated results using the kernels $U_{ij}^{*1}(\xi, x)$ and $U_{ij}^{*2}(\xi, x)$, and the exact results from the closed form solution are shown in Fig. 7, where (a) $g_1(\theta)_{ex}, g_2(\theta)_{ex}$ are from exact solution, or from the complex potentials Eq. (33) directly, (b) $g_1(\theta)_{*1}$ $g_2(\theta)_{*1}$ are from the usage of the kernels $U_{ij}^{*1}(\xi, x)$ and (c) $g_1(\theta)_{*2}$, $g_2(\theta)_{*2}$ are from the usage of the kernels $U_{ij}^{*2}(\xi, x)$.

It is found from Fig. 7 that, the computed results from the usage of the kernel $U_{ij}^{*1}(\xi, x)$ or $U_{ij}^{*2}(\xi, x)$, and those from the exact solution, are merged into the same curves.

Figs. 6,7

3. Numerical evaluations for degenerate scale problems for different kernels $U_{ij}^{*g}(\xi, x)$

Instead of two kernels $U_{ij}^{*1}(\xi, x)$ and $U_{ij}^{*2}(\xi, x)$, a kernel $U_{ij}^{*g}(\xi, x)$ in a more general form is defined as

$$U_{ij}^{*g}(\xi,x)=\frac{1}{8\pi(1-\nu)G}\left\{-(3-4\nu)\ln(r)\delta_{ij}+r_{,i}r_{,j}-s\delta_{ij}\right\} \quad (34)$$

where "s" can take any real value.

Clearly, a homogenous equation for the degenerate scale problem using the kernel $U_{ij}^{*g}(\xi,x)$ can be formulated

$$\int_{\Gamma_d} U_{ij}^{*g}(\xi,x)p_j(x)ds(x)=0\ , \quad (i=1,2,\ \xi\in\Gamma) \quad (35)$$

In the formulation, one want to find a particular size such that Eq. (35) has a non-trivial solution for $p_j(x)$, or $p_j(x)\neq 0$. By using relevant solutions in normal scale problem, the degenerate scale problem can be solved [Chen et al. 2005; Vodicka and Mantic 2008].

In a recent publication [Chen et al. 2009], after using two fundamental solutions in the normal scale, the degenerate scale problem can be solved. In this paper, the method suggested in [Chen et al. 2009] is used to solve the problems in Examples 5 and 6. Clearly, the degenerate scale must depend on the assumed constant "s" in Eq. (34).

Example 5

In the example, the ellipse has a major half-axis "a" and minor half-axis "b" (Fig.1(b)). In computation, the plane strain condition and $\nu=0.3$ are assumed. The elliptic contour is divided into 120 intervals. For the BIE solution, the constant displacement and traction are assumed for each interval. For the cases of (1) s=-0.5, 0, 0.5, 1.0 and 1.5, (2) b/a=0.1, 0.2,…1.0, two degenerate scales are expressed as

$$a_{d1}=f_1(s,b/a),\quad a_{d2}=f_2(s,b/a) \quad (36)$$

The computed results for $f_1(s,b/a)$ and $f_2(s,b/a)$ are listed in Table 1. From the tabulated results we see that if the value of "s" changes from –0.5, 0, 0.5, 1.0 to 1.5, the degenerate scale becomes smaller and smaller.

Example 6

In the example, the rectangular notch has a width "2a" and a height "2b" (Fig. 1(c)). Similarly, for the cases of: (1) s=-0.5, 0, 0.5, 1.0 and 1.5, (2) b/a=0.1, 0.2,…1.0, two degenerate scales are

expressed as

$$a_{d1} = g_1(s, b/a), \quad a_{d2} = g_2(s, b/a) \tag{37}$$

The computed results for $g_1(s, b/a)$ and $g_2(s, b/a)$ are listed in Table 2. Similar to the previous example, if the value of "s" changes from –0.5, 0, 0.5, 1.0 to 1.5, the degenerate scale becomes smaller and smaller

4. Conclusions

From the above-mentioned theoretical analysis and the numerical examinations we can get the following conclusions. The kernel $U_{ij}^{*1}(\xi, x)$ can be used to arbitrary loading on the contour. However, the $U_{ij}^{*2}(\xi, x)$ can only be used to the case that the loading on the contour must be in equilibrium. It is an effective way to examine a suggested BIE by using a known solution, particularly, through a solution expressed in the complex potentials. In this case, since the solution is known beforehand, and one can easily judge whether the formulation used in computation is correct or not.

In the case of using the kernel $U_{ij}^{*1}(\xi, x)$, properties of solutions form BIE are clearly studied. If the degenerate scale has not been reached, the Dirichlet problem has a unique solution. Generally, the computed tractions on the boundary may result in resultant forces along the contour. In the Neumann problem, the computed displacements must belong to the boundary values of the displacement field expressed in the pure deformable form.

In the degenerate scale problem, the constant "s" involved in the integral kernel $U_{ij}^{*g}(\xi, x)$ has a significant influence to the final results of degenerate scale.

References

[Brebbia et al 1984] C. A. Brebbia, J. C. F. Telles, L. C. Wrobel, *Boundary element techniques – theory and applications in engineering*, Springer, Heidelberg, 1984.

[Chen 2003] Y. Z. Chen, " Analysis of L-integral and theory of the derivative stress field in plane elasticity", *Inter. J Solids Struc.* **40** (2003), 3589-3602.

[Chen et al. 2002] J. T. Chen, S. R. Kuo, J. H. Lin, "Analytical study and numerical experiments for degenerate scale problems in the boundary element method of two-dimensional elasticity", *Int. J. Numer. Meth. Eng.* **54** (2002), 1669-1681.

[Chen et al. 2005] J. T. Chen, S. R. Lin, K. H. Chen, "Degenerate Scale problem when solving Laplace's equation by BEM and its treatment", *Int. J. Numer. Meh. Eng.* **62** (2005), 233-261.

[Chen and Shen 2007] J. T. Chen, W. C. Shen, "Degenerate scale for multiply connected Laplace problems", *Mech. Res. Commun.* **34** (2007), 69–77.

[Chen and Lin 2008] Y. Z. Chen, X. Y. Lin, "Regularity condition and numerical examination for degenerate scale problem of BIE for exterior problem of plane elasticity", *Eng. Anal. Bound. Elem.* **32** (2008), 811-823.

[Chen et al. 2009] Y. Z. Chen, X. Y. Lin, Z. X. Wang , "Numerical solution for degenerate scale problem for exterior multiply connected region", *Eng. Anal. Bound. Elem.* **33** (2009), 1316-1321.

[Cheng and Cheng 2005] A. H. D. Cheng, D.S. Cheng, "Heritage and early history of the boundary element method", *Eng. Anal. Bound. Elem.* **29** (2005), 286-302.

[Cruse 1969] T. A. Cruse, "Numerical solutions in three-dimensional elastostatics", *Inter. J. Solids Struc.* **5** (1969), 1259-1274.

[He et al. 1996] W. J. He, H. J. Ding, H. C. Hu, "Degenerate scale and boundary element analysis of two dimensional potential and elasticity problems", *Comput. Struct.* **60** (1996), 155-158.

[Jaswon and Symm 1977] M. A. Jaswon, G. T. Symm, *Integral equation methods in potential theory and elastostatics.* Academic Press, London, 1977.

[Muskhelishvili 1953] N. I. Muskhelishvili, *Some basic problems of mathematical theory of elasticity*, Noordhoof, Netherlands, 1953.

[Rizzo 1967] F. J. Rizzo, "An integral equation approach to boundary value problems in classical elastostatics", *Quart. J. Appl. Math.* **25** (1967), 83-95.

[Vodicka and Mantic 2008] R. Vodicka, V. Mantic, " On solvability of a boundary integral equation of the first kind for Dirichlet boundary value problems in plane elasticity", *Comput. Mech.* **41**

(2008), 817-826.

Table 1. The degenerate scale $a_{d1} = f_1(s, b/a)$ and $a_{d2} = f_2(s, b/a)$ for an eclipse notch (see Eq. (36) and Fig. 1(b))

$a_{d1} = f_1(s, b/a)$

b/a=	0.1	0.2	0.3	0.4	0.5	0.6	0.7	0.8	0.9	1.0
s=										
-0.5	2.52541	2.41447	2.30954	2.21105	2.11897	2.03305	1.95295	1.87824	1.80853	1.74340
0.	1.91291	1.82888	1.74940	1.67479	1.60504	1.53997	1.47929	1.42270	1.36990	1.32057
0.5	1.44896	1.38531	1.32511	1.26860	1.21577	1.16647	1.12051	1.07765	1.03765	1.00028
1	1.09754	1.04932	1.00372	0.96092	0.92090	0.88356	0.84875	0.81628	0.78598	0.75768
1.5	0.83135	0.79483	0.76029	0.72786	0.69755	0.66927	0.64290	0.61830	0.59535	0.57392

$a_{d2} = f_2(s, b/a)$

b/a=	0.1	0.2	0.3	0.4	0.5	0.6	0.7	0.8	0.9	1.0
s=										
-05	3.97868	3.49681	3.11489	2.80545	2.55005	2.33597	2.15411	1.99784	1.86219	1.74340
0	3.01371	2.64871	2.35942	2.12503	1.93158	1.76942	1.63166	1.51329	1.41054	1.32057
0.5	2.28278	2.00631	1.78718	1.60963	1.46310	1.34027	1.23593	1.14627	1.06844	1.00028
1.0	1.72913	1.51971	1.35373	1.21924	1.10825	1.01521	0.93617	0.86826	0.80930	0.75768
1.5	1.30975	1.15112	1.02540	0.92353	0.83946	0.76899	0.70912	0.65767	0.61302	0.57392

Table 2. The degenerate scale $a_{d1} = g_1(d, b/a)$ and $a_{d2} = g_2(d, b/a)$ for a rectangular notch (see Eq. (37) and Fig. 1(c))

$a_{d1} = g_1(s, b/a)$

b/a=	0.1	0.2	0.3	0.4	0.5	0.6	0.7	0.8	0.9	1.0
s=										
-0.5	2.40472	2.22301	2.07631	1.95320	1.84796	1.75521	1.67343	1.60015	1.53398	1.47394
0.	1.82149	1.68385	1.57273	1.47948	1.39977	1.32951	1.26756	1.21206	1.16194	1.11646
0.5	1.37971	1.27546	1.19129	1.12066	1.06028	1.00706	0.96014	0.91809	0.88013	0.84568
1	1.04508	0.96612	0.90236	0.84886	0.80312	0.76281	0.72727	0.69542	0.66666	0.64057
1.5	0.79162	0.73180	0.68351	0.64298	0.60834	0.57780	0.55088	0.52676	0.50498	0.48521

$a_{d2} = g_2(s, b/a)$

b/a=	0.1	0.2	0.3	0.4	0.5	0.6	0.7	0.8	0.9	1.0
s=										
-0.5	3.61122	3.04801	2.66064	2.37149	2.14534	1.96172	1.80951	1.68074	1.57017	1.47394
0.	2.73537	2.30876	2.01534	1.79632	1.62502	1.48593	1.37064	1.27310	1.18935	1.11646
0.5	2.07195	1.74881	1.52655	1.36065	1.23090	1.12554	1.03821	0.96433	0.90089	0.84568
1	1.56943	1.32466	1.15631	1.03065	0.93236	0.85256	0.78641	0.73045	0.68239	0.64057
1.5	1.18879	1.00338	0.87587	0.78068	0.70623	0.64578	0.59568	0.55329	0.51689	0.48521

Captions of Figures

Fig. 1 (a) A concentrated force applied at the point z=t, or the loading condition for the $\alpha-$ field, (b) Some loadings having resultant forces applied on the elliptic contour, or the loading condition for the $\beta-$ field or the physical stress field. (c) A rectangular notch.

Fig. 2 Non-dimensional displacements for an exterior problem with the non-equilibrium loadings on contour, (a) $f_1(\theta)_{ex}$, $f_2(\theta)_{ex}$ from the exact solution, (b) $f_1(\theta)_{*1}$, $f_2(\theta)_{*1}$ by using the kernel $U_{ij}^{*1}(\xi, x)$ (c) $f_1(\theta)_{*2}$, $f_2(\theta)_{*2}$ by using $U_{ij}^{*2}(\xi, x)$ in the case of b/a=0.25, a=40, $A_1 = 1$ $A_2 = 0.5$ in Eq. (29) (see Fig. 1(b) and Eq. (31))

Fig. 3 Non-dimensional displacements for an exterior problem with the non-equilibrium loadings on contour, (a) $f_1(\theta)_{ex}$, $f_2(\theta)_{ex}$ from the exact solution, (b) $f_1(\theta)_{*1}$, $f_2(\theta)_{*1}$ by using the kernel $U_{ij}^{*1}(\xi, x)$ (c) $f_1(\theta)_{*2}$, $f_2(\theta)_{*2}$ by using $U_{ij}^{*2}(\xi, x)$ in the case of b/a=0.25, a=4, $A_1 = 1$ $A_2 = 0.5$ in Eq. (29) (see Fig. 1(b) and Eq. (31))

Fig. 4 Non-dimensional tractions for an exterior problem with the non-equilibrium loadings on contour, (a) $g_1(\theta)_{ex}$, $g_2(\theta)_{ex}$ from the exact solution, (b) $g_1(\theta)_{*1}$, $g_2(\theta)_{*1}$ by using the kernel $U_{ij}^{*1}(\xi, x)$ (c) $g_1(\theta)_{*2}$, $g_2(\theta)_{*2}$ by using $U_{ij}^{*2}(\xi, x)$ in the case of b/a=0.25, a=40, $A_1 = 1$ $A_2 = 0.5$ in Eq. (29) (see Fig. 1(b) and Eq. (32)).

Fig. 5 Non-dimensional tractions for an exterior problem with the non-equilibrium loadings on contour, (a) $g_1(\theta)_{ex}$ $g_2(\theta)_{ex}$ from the exact solution, (b) $g_1(\theta)_{*1}$ $g_2(\theta)_{*1}$ by using the kernel $U_{ij}^{*1}(\xi, x)$ (c) $g_1(\theta)_{*2}$ $g_2(\theta)_{*2}$ by using $U_{ij}^{*2}(\xi, x)$ in the case of b/a=0.25, a=4, $A_1 = 1$ $A_2 = 0.5$ in Eq. (29) (see Fig. 1(b) and Eq. (32)).

Fig. 6 Non-dimensional displacements for an exterior problem with the non-equilibrium loadings on contour , (a) $f_1(\theta)_{ex}$, $f_2(\theta)_{ex}$ from the exact solution, (b) $f_1(\theta)_{*1}$ $f_2(\theta)_{*1}$ by using the kernel $U_{ij}^{*1}(\xi, x)$ (c) $f_1(\theta)_{*2}$ $f_2(\theta)_{*2}$ by using $U_{ij}^{*2}(\xi, x)$ in the case of b/a=0.25, a=4, $A_1 = 1$, $A_2 = 0.5$, $B_1 = 1$, $B_2 = 0.5$ in Eq. (33) (see Fig. 1(b) and Eq. (31)).

Fig. 7 Non-dimensional tractions for an exterior problem with the non-equilibrium loadings on contour , (a) $g_1(\theta)_{ex}$, $g_2(\theta)_{ex}$ from the exact solution, (b) $g_1(\theta)_{*1}$ $g_2(\theta)_{*1}$ by using the kernel $U_{ij}^{*1}(\xi, x)$ (c) $g_1(\theta)_{*2}$ $g_2(\theta)_{*2}$ by using $U_{ij}^{*2}(\xi, x)$ in the case of b/a=0.25, a=4, $A_1 = 1$ $A_2 = 0.5$, $B_1 = 1$, $B_2 = 0.5$ in Eq. (33) (see Fig. 1(b) and Eq. (32)).

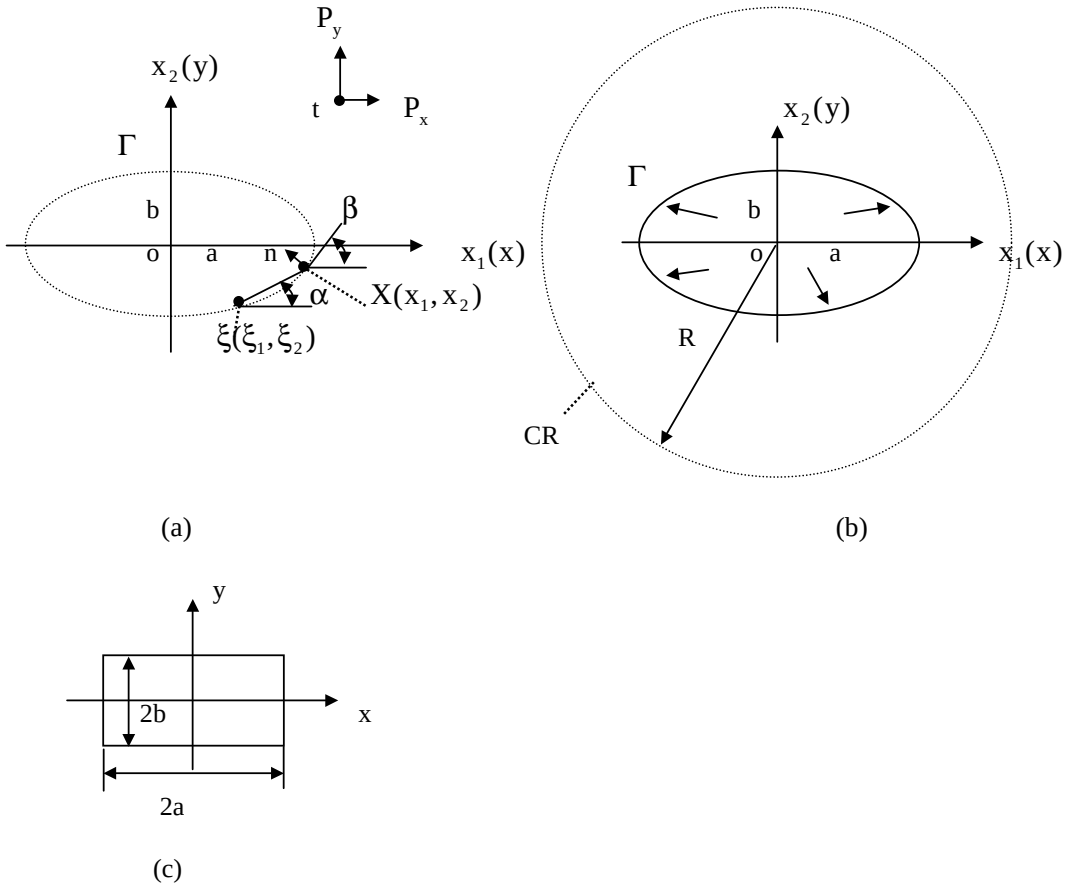
P_y
x_2(y)
t
P_x
Γ
b
β
o
a
n
x_1(x)
α
X(x_1, x_2)
ξ(ξ_1, ξ_2)
x_2(y)
Γ
b
o
a
x_1(x)
R
CR
(a)
(b)
y
2b
x
2a
(c)

Fig. 1

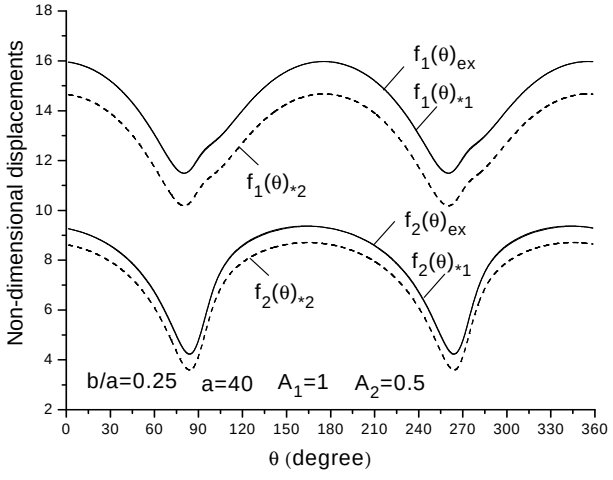
Non-dimensional displacements
θ (degree)
f_1(θ)_ex
f_1(θ)_*1
f_1(θ)_*2
f_2(θ)_ex
f_2(θ)_*1
f_2(θ)_*2
b/a=0.25
a=40
A_1=1
A_2=0.5

Fig. 2

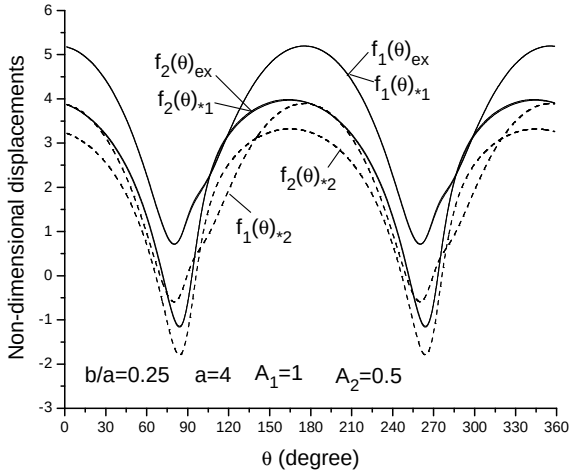
Non-dimensional displacements
θ (degree)
$f_2(\theta)_{ex}$
$f_1(\theta)_{ex}$
$f_2(\theta)_{*1}$
$f_1(\theta)_{*1}$
$f_2(\theta)_{*2}$
$f_1(\theta)_{*2}$
b/a=0.25 a=4 A_1=1 A_2=0.5

Fig. 3

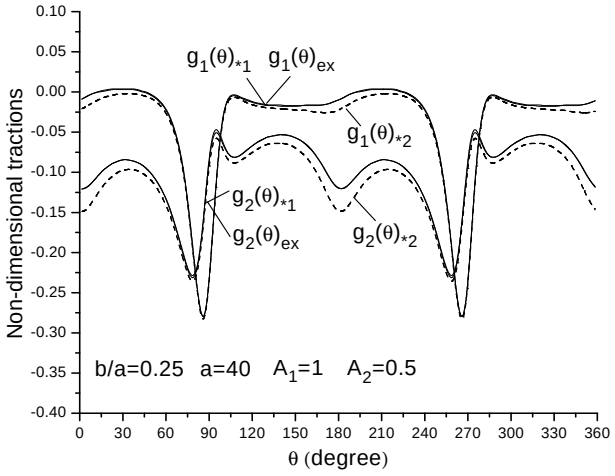
Non-dimensional tractions
θ (degree)
$g_1(\theta)_{*1}$ $g_1(\theta)_{ex}$
$g_1(\theta)_{*2}$
$g_2(\theta)_{*1}$
$g_2(\theta)_{ex}$
$g_2(\theta)_{*2}$
b/a=0.25 a=40 A_1=1 A_2=0.5

Fig. 4

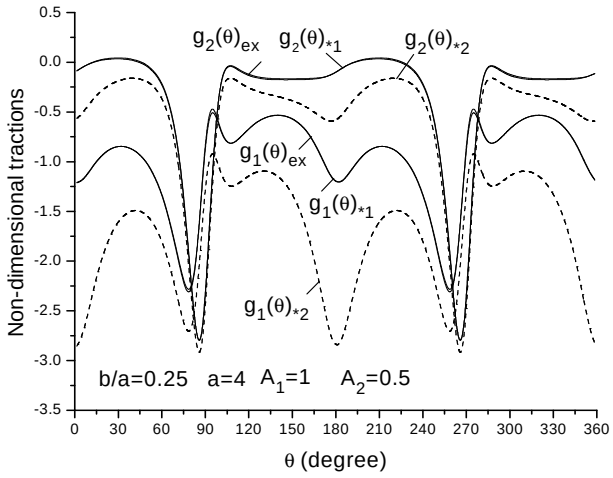
Non-dimensional tractions
θ (degree)
g2(θ)ex
g2(θ)*1
g2(θ)*2
g1(θ)ex
g1(θ)*1
g1(θ)*2
b/a=0.25 a=4 A1=1 A2=0.5

Fig. 5

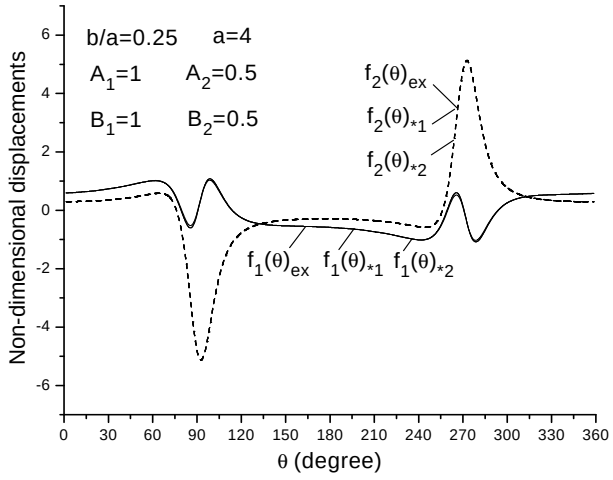
Non-dimensional displacements
θ (degree)
b/a=0.25 a=4
A1=1 A2=0.5
B1=1 B2=0.5
f2(θ)ex
f2(θ)*1
f2(θ)*2
f1(θ)ex
f1(θ)*1
f1(θ)*2

Fig. 6

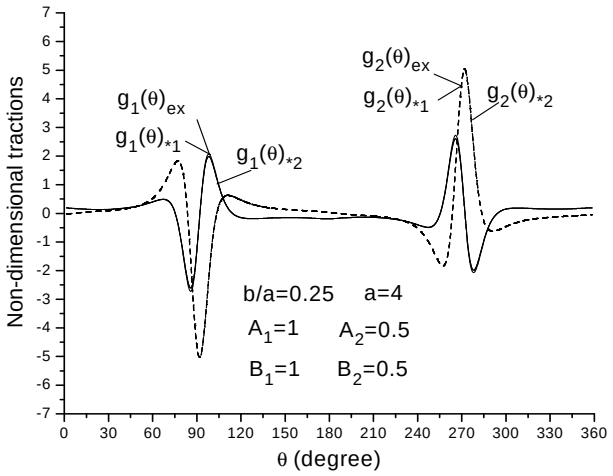
Non-dimensional tractions
θ (degree)
$g_1(\theta)_{ex}$
$g_1(\theta)_{*1}$
$g_1(\theta)_{*2}$
$g_2(\theta)_{ex}$
$g_2(\theta)_{*1}$
$g_2(\theta)_{*2}$
b/a=0.25 a=4
A_1=1 A_2=0.5
B_1=1 B_2=0.5

Fig.7